Published in final edited form as:
*Haptics (2014)*. 2014 ; 2014: 360–368. doi:10.1007/978-3-662-44196-1_44.

# Computational Modeling Reinforces that Proprioceptive Cues May Augment Compliance Discrimination When Elasticity Is Decoupled From Radius of Curvature

**Yuxiang Wang** and **Gregory J. Gerling**[*]
Departments of Systems and Information Engineering, and Mechanical and Aerospace Engineering, University of Virginia, Charlottesville, VA 22903, USA

## Abstract

Our capability to discriminate object compliance is based on cues both tactile and proprioceptive, in addition to visual. To understand how the mechanics of the fingertip skin and bone might encode such information, we used finite element models to simulate the task of differentiating spherical indenters of radii (4, 6 and 8 mm) and elasticity (initial shear modulus of 10, 50 and 90 kPa). In particular, we considered two response variables, the strain energy density (SED) at the epidermal-dermal interface where Merkel cell end-organs of slowly adapting type I afferents reside, and the displacement of the fingertip bone necessary to achieve certain surface contact force. The former variable ties to tactile cues while the latter ties to proprioceptive cues. The results indicate that distributions of SED are clearly distinct for most combinations of object radii and elasticity. However, for certain combinations – e.g., between 4 mm spheres of 10 kPa and 8 mm of 90 kPa – spatial distributions of SED are nearly identical. In such cases where tactile-only cues are non-differentiable, we may rely on proprioceptive cues to discriminate compliance.

### Keywords

Haptics; softness; compliance; perception; finite element analysis; touch; tactile; proprioception; mechanotransduction; biomechanics

## 1 Introduction

In daily interactions with our environment, we classify the compliance of objects as soft or hard, or at levels in-between. The percept of compliance, despite its importance, is much less studied and understood than is the case for rigid bodies. It is also much less studied for bare finger interaction [1, 2] (e.g., palpation of cancerous nodules) than for probe-based interaction [3, 4] (e.g., simulation of detection of caries). Accordingly, work herein focuses upon bare finger interaction, and employs computational modeling to better understand the relative contributions of the fingertip skin and bone in encoding compliance.



[*]yw5aj@virginia.edu.
gg7h@virginia.edu


NIH-PA Author Manuscript
NIH-PA Author Manuscript

To inform a percept of compliance, our somatosensory system senses, transforms and integrates various types of cues, both tactile and proprioceptive [1, 3], in addition to visual. Tactile cues arise from interactions between the fingertip skin and an object's surface whereby mechanosensitive afferents respond to spatial and temporal distributions of stress and strain fields in skin near their end organs. We rely almost exclusively upon tactile cues in passive touch. In contrast, in situations of active exploration, we augment tactile cues with proprioceptive cues from the movement of our fingers in space. Employing both systems together, in active touch, leads to peak performance. When finger movement cues are removed, our ability to discriminate compliance decreases [1]. Likewise, when tactile cues are removed (by an experimental setup that has the user grasp two rigid plates with the elastic substrate in-between), our ability to discriminate compliance decreases by more than three times [2].

To better understand the relative contributions of tactile and proprioceptive cues in discriminating compliance, stimulus elasticity needs to be decoupled from its radius of curvature. In specific, prior work has been conducted, but with stimuli whose properties were confounded as follows. First, stimulus compliance has been parameterized by its stiffness (force-displacement, units N/m) rather than its elastic modulus (stress-strain, units Pa) [1]. This is an issue because two stimuli can maintain equal stiffness yet differ in elasticity when accounting for size and surface geometry. Second, stimuli often employ a flat, rigid surface with a spring under the surface that controls compliance [2–4]. Such stimuli do not mimic the contact profile of an elastic object and the skin's surface. Third, others employ stimuli that correctly characterize compliance by elastic modulus and account for elastic-to-elastic surface contact, but only use stimuli of flat surface geometry. Finally and relatedly, single-nerve, electrophysiological recordings have recently been conducted in response to compliant stimuli [5, 6]. To fill the gap between single-unit recordings and psychophysical studies, computational models are required to decipher how a population of afferents encodes compliance. The modeling herein is a first step toward identifying parameters to be used to drive further, and more conclusive, psychophysical experiments.

We address this gap in the knowledge base by computationally modeling the mechanics of both the fingertip skin and bone and conducting numerical experiments where stimulus elasticity is decoupled from radius of curvature. We utilize control conditions that simulate active and passive touch and approximate tactile and proprioceptive cues. In the analysis of cutaneous tactile cues, we focus in this work upon the steady-state phase of the indentation, which is tied with the response of the slowly-adaptive type I afferent, as opposed to other afferent types.

## 2 Methods

Finite element analysis of the skin and bone of the distal fingertip was performed using both plane-strain and axisymmetric models. Their material properties were fitted to hyperelastic material constitutive laws, and optimized to predict known surface deflection and force-displacement relationships. Then, a series of numerical simulations were carried out with compliant spherical indenters of different radii (4, 6 and 8 mm) and elasticity (initial shear modulus of 10, 50 and 90 kPa). In two interaction cases, the fingertip and stimulus are moved and constrained in attempt to approximate active and passive touch. To help determine stimulus discriminability, two response variables were considered at steady-state fingertip-stimulus contact, the strain energy density (SED) at the epidermal-dermal interface where Merkel cell end-organs of slowly adapting type I afferents reside, and displacement of the fingertip bone necessary to achieve certain contact force. The first variable directly ties to cutaneous or tactile-only cues. The second variable ties to proprioceptive cues, where displacement of the bone in the normal direction is an approximate measure tied to change in muscle length, and force tied to muscle tension change.

### 2.1 Geometry of the fingertip model

Derived from the geometry of a 3D model of the human distal phalange [7], the two simplified 2D models with plane-strain elements (Fig. 1A) of a cross-sectional slice from proximal first digit to distal tip, to account for stimuli delivered across the width of the finger (e.g., bars), and with axisymmetric elements (Fig. 1B) revolved around the centerline of the fingerpad, to analyze stimuli normal to the contact surface (e.g., spherical and cylindrical indenters). Herein, the plane strain model was used to fit material properties to surface deflection data [8], while the axisymmetric model was used to fit force-displacement data [9] and perform simulations with compliant spherical objects. The simplified 2D models are of much less computational expense, necessary as the parametric study herein included a considerable number of model evaluations.

The bones and fingernails in the models are analytic rigid bodies, as these structures are much stiffer than soft tissue. The fingernail is 0.46 mm thick and 13 mm long. Three layers of soft tissue were modeled as deformable bodies wrapped around the bone, namely epidermis, dermis and hypodermis. Layers interface were tied with no relative displacements.

Meshing was done with elements near the surface of the finest dimension, about 0.25 mm wide, with larger sizes gradually used closer to the bone. Triangular meshes were used throughout with 4,032 and 3,456 elements in the plane-strain and axisymmetric models.

### 2.2 Material properties of the fingertip model

Hyperelastic material properties are used of the Neo-Hookean form of the strain energy func-tion, Eqn. 1. Specifically, $\Psi$ is the strain energy term, $\bar{I}_1$ is the modified first strain invariant, $J$ is the strain energy term, is the volume ratio known as Jacobian and $C_{10}$, $D_1$are material constants [10].

$$\Psi = C_{10}\left(\bar{I}_1 - 3\right) + \frac{1}{D_1}(J-1)^2 \quad (1)$$

The initial shear modulus $G$ was first defined and then initial bulk modulus was set according to $K = G10^5$. The relationship between parameters $G$, $K$ and terms in strain energy function $C_{10}$ and $D_1$ is $G = 2C_{10}$ and $K = \frac{2}{D_1}$.

We refer to material elasticity by its initial shear modulus (denoted as G), which fully defines the material. Though we specify elasticity only via the linear term G, the material is in fact nonlinearly hyperelastic. The purpose of choosing Neo-Hookean model is two-fold. First, only one parameter is needed (G) for each material, thereby simplifying the fitting procedure and leading to a more robust calibration. Second, instead of a linear Young's modulus, we use a hyperelastic form because we focus on soft objects, which deform in a finite-strain region.

In addition, a two-step model material calibration was conducted. First, the ratios between material elasticity of each layer were fitted to plane strain model to match observed spatial deflection of the fingertip surface to different displacements of different cylinders [8]. Second, the ratios were scaled in the axisymmetric model to match observed force-displacement relationships from four subjects [9]. The material parameters obtained from the fitting procedures are listed in Table 1. The final values of shear modulus G are epidermis 1.21 MPa, dermis 50.67 kPa and hypodermis 2.37 kPa. A friction coefficient between simulated skin and stimulus is set to 0.3 [11]. The models were constructed and analyzed using the commercial FE software package ABAQUS Standard, version 6.12 (Dassault Systèmes, Vélizy-Villacoublay, France).

### 2.3 Modeled indenter tips

The set of compliant spherical indenters utilize three values of radii (4, 6 and 8 mm) and elasticity (initial shear modulus of 10, 50 and 90 kPa). The indenters are implemented as hemispheres, with the surface of their central section tied to a rigid plate. Their Poisson's ratio is set to 0.475 to mimic the nearly incompressible behavior of rubber. Triangular elements with 0.25 mm edge length are used because their size is comparable to elements used in the fingertip model in the region contacting its surface, for the purpose of suppressing stress concentrations near nodes. Larger elements of up to 1.0 mm are used to reduce computational cost in the region not directly contacting the skin.

### 2.4 Numerical experiments

Nine numerical simulations (3 radii by 3 elasticity) were conducted on the 2D axisymmetric model. Two types of fingertip-stimulus contact and movement were simulated, tied to cases of active and passive touch. First, in the passive touch case (Fig. 2A), all compliant indenters regardless of size and material were loaded by 0.125, 0.25, 0.5 and 1 N force, while the fingertip bone was constrained. The response variables in the passive touch case were derived from tactile-only cues, indicated by the SED distributed on nodes at the simulated epidermal-dermal interface (470 μm beneath the skin's surface) calculated by averaging neighboring elements at each interface node. With the bone fixed, we assumed no proprioceptive cues as reaction force is provided by fixture instead of muscle activity. Second, in the active touch case (Fig. 2B), all compliant indenters were constrained at the center plate while the fingertip bone was loaded by the noted forces. The response variables in the active touch case were derived from both tactile and proprioceptive cues. The additional proprioceptive cues were derived from the translational displacement of the fingertip bone in the normal direction. This is a measure that ties to the change in the length of the muscle as detected by muscle spindles whereas the corresponding force indicates the muscle tension change of Golgi tendons [12]. Note that under both cases the SED distributions are identical due to the same loading magnitude.

## 3 Result

At a first glance, the indenters deform the surface of the skin quite distinctly given changes in either radius or elasticity (Fig. 3).

For tactile-only cues, either a decrease in spherical radius or an increase in material elasticity (decrease in compliance) will significantly increase the concentration of SED near the contact centerline (Fig. 4). Therefore most differences of the indenter can be clearly captured and discriminated by comparing such curves. In certain cases, however, changes in elasticity may perfectly counteract changes in radius. In particular, the distribution of SED for the smallest radius, most compliant case (Fig. 4A) is nearly identical to that of the largest radius, least compliant case (Fig. 4E), as combined in Fig. 4F.

For proprioceptive cues, an increase in either indenter radius or elasticity will lead to a decrease in the displacement of the bone given the same force (Fig. 5). For example, in Fig. 5 the dotted line (G = 10 kPa, r = 4 mm) is clearly separable from the solid line with dot markers (G = 90 kPa, r = 8 mm). Also, curves differing by indenter radius (r = 4, 6, 8 mm) with the same elasticity (G = 10 kPa) yield a similar relationship. In contrast, curves differing by elasticity (G = 10, 50 kPa) the same radius (r = 8 mm) yield a much more distinct relationship.

## 4 Discussion

We computationally modeled the mechanics of both the fingertip skin and bone and conducted numerical experiments where stimulus elasticity was decoupled from radius of curvature. In two interaction cases, the fingertip and stimulus were moved and constrained in attempt to approximate active and passive touch. Response variables were tied to tactile and proprioceptive mechanisms of spatial distributions of SED and the displacement of the distal bone.

The results indicate that the tactile cues appear to more readily aid discriminating compliant objects, because of the clear separation of SED distributions (Fig. 4) compared to differences in the displacement of the bone in the normal direction, which we use to approximate proprioceptive cues (Fig. 5). In specific, the models predict that one might observe a tactile illusion in situations where proprioceptive cues are absent (e.g., in the passive touch case), when stimulating with spheres of 4 mm of 10 kPa versus 8 mm of 90 kPa, where one might be unable to differentiate the two spheres. However, adding the simulated proprioceptive cues enabled us to discriminate these cases. This result reinforces that, and provides a specific instance where, both tactile and proprioceptive cues might be jointly relied upon to discriminate compliant objects. This comes in general agreement with psychophysical studies where Bergmann Tiest et al. reported lower discrimination ability based on proprioceptive cues alone compared to tactile cues alone [2], and Srinivasan et al. reported that tactile cues encode more information than proprioceptive cues [1]. However, as we noted in the introduction those experiments were conducted in situations where stimulus compliance and/or surface contact were confounded together or ill defined.

While the effort here is a first attempt to decouple stimulus elasticity from radius of curvature, further work is needed to account for assumptions made herein. First, our FE analyses are done in steady-state and do not take material viscoelasticity into account. This time-varying information is likely to contribute to the response characteristics of both rapid-adapting and slowly-adapting type I afferents [5, 13], and it is likely that the timing of the action potentials in the stimulus ramp contribute to compliance discrimination [5]. Second, the spherical indenter used herein does not shed any light on how distinct spatial features, such as edges, might be encoded apart from material compliance. Third, several assumptions are made with respect to the proprioceptive cues we utilized. We use displacement and force in the normal direction as a first approximation, though cues might also be transferred to change in muscle length and tension. One may need to simulate the next phalange of the finger as well as consider the exact connectivity of the muscles and tendons to the bone at points in the finger digits. Fourth, an often-considered tactile cue for designing haptic displays [14], distinct from stress/strain at the locations of the SAI end organs, is the deflection of the skin's surface. Though less clearly tied to the neurophysiology, our preliminary analysis is similar to the spatial distribution of SED. Another prominent cue, the spread of the contact area, can be analyzed in detail by calculating the area on the finger where SED is observed to be greater than a certain threshold. Finally, further psychophysical experiments are required to validate the simulated results, in particular the hypothesized illusion, and the values of radii and elasticity provide a good starting point.

## Supplementary Material

Refer to Web version on PubMed Central for supplementary material.

## Acknowledgements

This work was supported by a grant from the National Institutes of Health (NIH NINDS R01NS073119). The content is solely the responsibility of the authors and does not necessarily represent the official views of the NIH.

## References

1. Srinivasan MA, LaMotte RH. Tactual discrimination of softness. J Neurophysiol. 1995; 73:88–101. [PubMed: 7714593]
2. Bergmann Tiest WM, Kappers A. Cues for haptic perception of compliance. IEEE Trans Haptics. 2009; 2:189–199. doi: 10.1109/TOH.2009.16.
3. Friedman RM, Hester KD, Green BG, LaMotte RH. Magnitude estimation of softness. Exp Brain Res. 2008; 191:133–42. doi: 10.1007/s00221-008-1507-5. [PubMed: 18679665]
4. LaMotte RH. Softness discrimination with a tool. J Neurophysiol. 2000; 83:1777–1786. [PubMed: 10758090]
5. Condon M, Birznieks I, Hudson K, et al. Differential sensitivity to surface compliance by tactile afferents in the human fingerpad. J Neurophysiol. 2013 doi: 10.1152/jn.00589.2013.
6. Gwilliam JC, Yoshioka T, Okamura AM. Hsiao SS Neural coding of passive lump detection in compliant artificial tissue. J. Neurophysiol. in press.
7. Gerling GJ, Rivest II, Lesniak DR, et al. Validating a population model of tactile mechanotransduction of slowly adapting type I afferents at levels of skin mechanics, single-unit response and psychophysics. IEEE Trans Haptics. 2013:1–1. doi: 10.1109/TOH.2013.36.
8. Dandekar K. Role of mechanics in tactile sensing of shape. 1995

9. Gulati RJ, Srinivasan MA. Human fingerpad under indentation I: static and dynamic force response. ASME-Publications-Bed. 1995; 29:261.
10. Holzapfel G. Nonlinear solid mechanics: A continuum approach for engineering. 2000
11. Gitis N, Sivamani R. Tribometrology of skin. Tribol Trans. 2004; 47:461–469. doi: 10.1080/05698190490493355.
12. Proske U, Gandevia SC. The proprioceptive senses: their roles in signaling body shape, body position and movement, and muscle force. Physiol Rev. 2012; 92:1651–97. doi: 10.1152/physrev.00048.2011. [PubMed: 23073629]
13. Johnson K. The roles and functions of cutaneous mechanoreceptors. Curr Opin Neurobiol. 2001; 11:455–461. doi: 10.1016/S0959-4388(00)00234-8. [PubMed: 11502392]
14. Bicchi A, Scilingo EP, De Rossi D. Haptic discrimination of softness in teleoperation: the role of the contact area spread rate. IEEE Trans Robot Autom. 2000; 16:496–504. doi: 10.1109/70.880800.

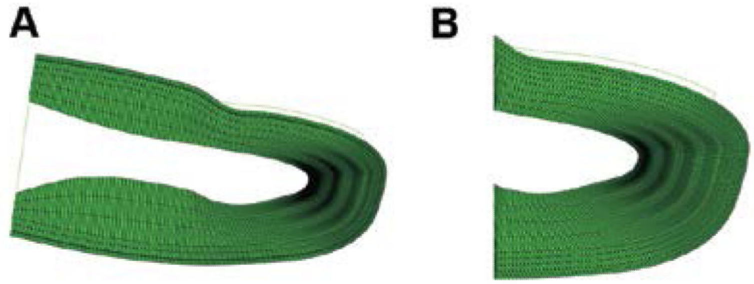


**Fig. 1.**
A) Plane-strain and B) axisymmetric models, following the geometry of the human distal phalange [7].

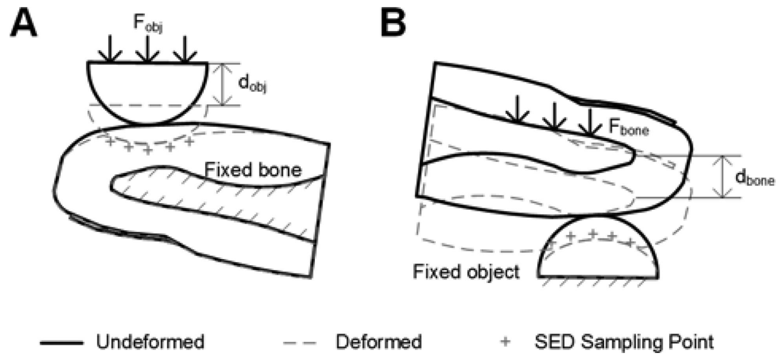


**Fig. 2.**

Forces and constraints in simulated cases of passive touch A) and active touch B), with the undeformed fingertip and compliant hemisphere denoted by dark, thick solid lines, and the deformed fingertip and compliant hemisphere by grey, thin dashed lines. Tactile cues in both A) and B) are simulated by measuring the spatial distribution of SED at elements at the epidermal-dermal interface (marked as "+") and proprioceptive cues in B) only are simulated by measuring the displacement of the bone $d_{bone}$, given force load $F_{bone}$ and the hyperelastic-tohyperelastic contact interaction.

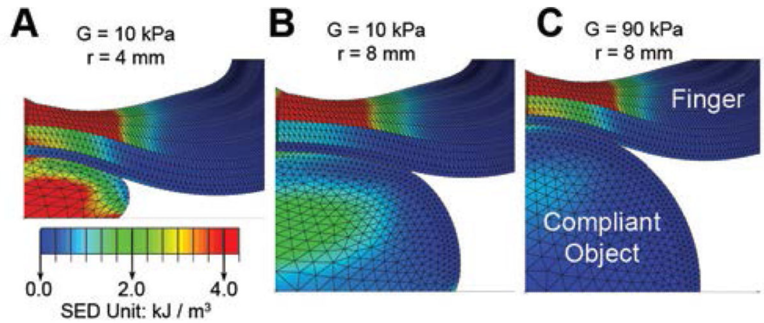


**Fig. 3.**

Contour plot of the spatial distribution of SED in the axisymmetric fingertip model (upper) at steady-state for simulated contact with compliant spheres (lower) varying in radii r and elasticity G, with A) smallest radius, most compliant, B) largest radius, most compliant, and C) largest radius, least compliant. Although the deformation of the spherical indenters differs vastly between A) and C), the surface deflection and the distribution of SED induced in the fingertip model are very similar.


NIH-PA Author Manuscript
NIH-PA Author Manuscript

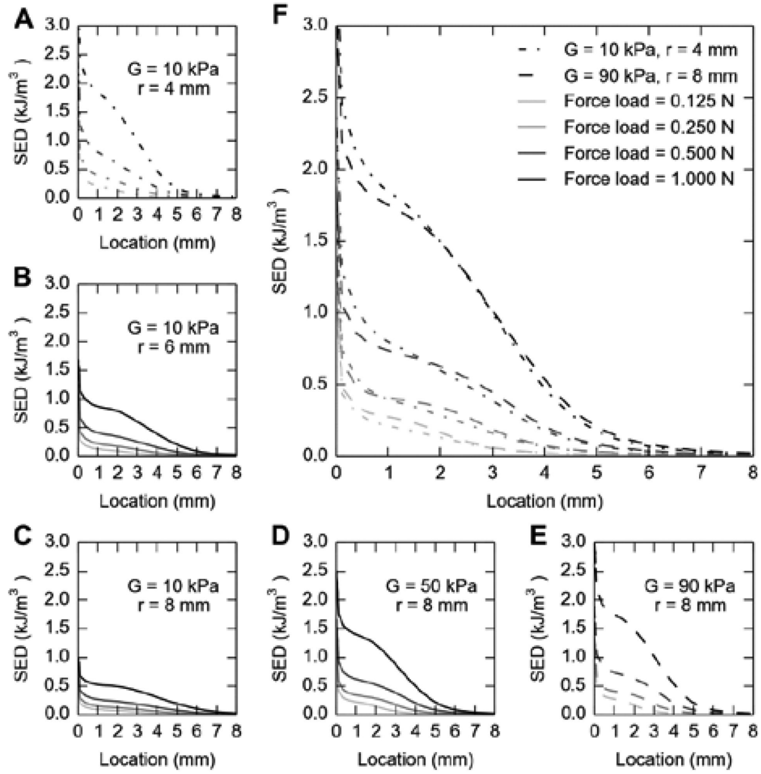


**Fig. 4.**

Simulated spatial distribution of SED in the axisymmetric fingertip model for spherical indenters varying in radii r and elasticity G, where shown in sub-figures are A-C) SED for indenter material G = 10 kPa and increasing radii from 4 mm to 8 mm, C-E) SED for indenters with equal radii of 8 mm and increasing elasticity from G = 10 kPa to 90 kPa, and F) the direct comparison of A) and E), demonstrating that the smallest radius, most compliant case in A) may be confused with largest radius, least compliant case in E) given SED distributions alone.

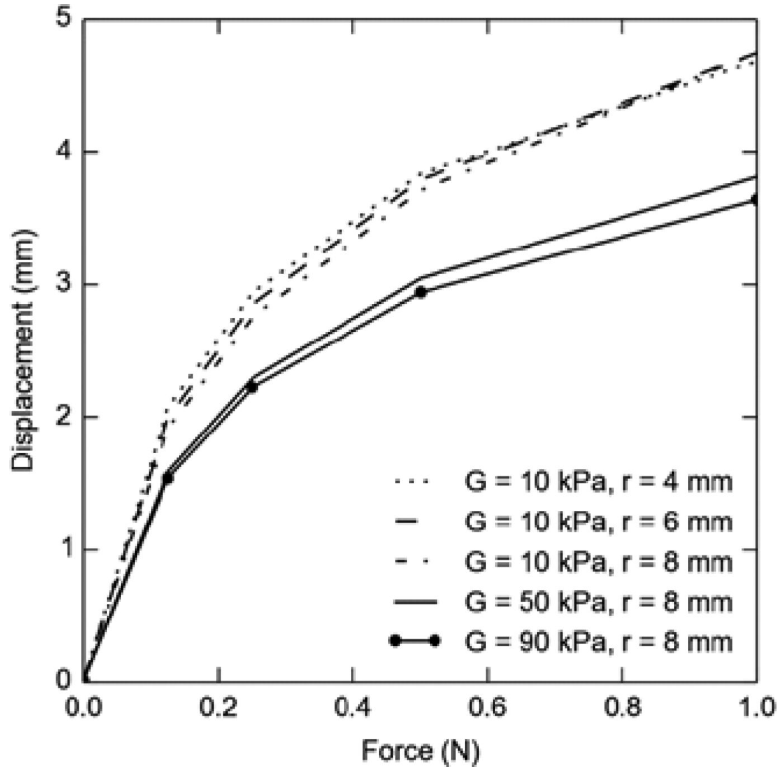


**Fig. 5.**
Displacement-force relationships of the bone simulated in the axisymmetric model of the fingertip are given for five combinations of indenter radii and elasticity.

NIH-PA Author Manuscript

NIH-PA Author Manuscript

## Table 1

Material parameters from fitting

| Subject | Initial shear modulus | | | $R^2$ |
|---|---|---|---|---|
| | **Epidermis (MPa)** | **Dermis (kPa)** | **Hypodermis (kPa)** | |
| #1 | 1.74 | 72.74 | 3.40 | 0.99 |
| #2 | 0.83 | 34.61 | 1.62 | 0.99 |
| #3 | 1.31 | 54.96 | 2.57 | 0.99 |
| #4 | 0.97 | 40.48 | 1.90 | 0.97 |
| **Mean** | **1.21** | **50.67** | **2.37** | **0.99** |
| Std. | 0.41 | 17.00 | 0.80 | 0.01 |